Gate-tunable optical filter based on conducting oxide metasurface heterostructure

JINQIANNAN ZHANG,[1,2,3] LONG TAO,[1] ALEKSEI ANOPCHENKO,[1] JINGYI YANG,[1] MICHAEL SCHELL,[1] ZHONGYUAN YU,[3] HO WAI HOWARD LEE[1,4,*]

[1]*Department of Physics, Baylor University, Waco, TX 76798, United States*
[2]*China Science and Technology Exchange Center, Beijing 10045, China*
[3]*State Key Laboratory of Information Photonics and Optical Communications, Beijing University of Posts and Telecommunications, Beijing 100876, China*
[4]*The Institute for Quantum Science and Engineering, Texas A&M University College Station, TX 77843, United States*
**Corresponding author: Howard_Lee@Baylor.edu*

Received XX Month XXXX; revised XX Month, XXXX; accepted XX Month XXXX; posted XX Month XXXX (Doc. ID XXXXX); published XX Month XXXX

A gate-tunable plasmonic optical filter incorporating a subwavelength patterned metal-insulator-metal (MIM) metasurface heterostructure is demonstrated. An additional thin transparent conducting oxide layer is embedded in the insulator layer to form a double metal-oxide-semiconductor (MOS) configuration. Heavily n-doped indium tin oxide (ITO) is used as the TCO material, whose optical property can be electrically tuned by the formation of a thin active epsilon-near-zero layer at the ITO-oxide interfaces. Full wave electromagnetic simulations show that 20 dB modulation strength is achievable with 4 V applied bias. This work is an essential step toward a realization of next-generation compact photonic/plasmonic integrated devices. © 2018 Optical Society of America

OCIS codes: *(050.6624) Subwavelength structures; (160.2100) Electro-optical materials; (160.3918) Metamaterials; (250.5403) Plasmonics.*

http://dx.doi.org/10.1364/OL.99.099999

Metamaterials are of great interest due to their exceptional performance in manipulating electromagnetic waves at optical frequencies. Compared to the conventional bulk metamaterials, metasurfaces - surface equivalent of metamaterials - can control light with flat optical structures less than a wavelength thick [1, 2]. Plasmonic metasurfaces are metallic nanostructures composed of periodic holes, slits, or resonator arrays in subwavelength scale which show distinct optical behaviors at plasmonic resonance. To date, the applications of plasmonic metasurfaces include flat lenses [3, 4], sensors [5, 6], wave plates [7, 8], polarizers [9], and color filters [10-15]. Among these applications, color filters have been a long-lasting focus of interest for ultracompact integrated photonic systems. However, for a given material with fixed intrinsic optical properties, the response of the filter could not be altered once it is fabricated. Several attempts have been carried out to dynamically modulate the phase or amplitude of the transmitted/reflected light of metasurfaces, which includes using a mechanical altering mechanism [16] or thermal [17, 18], optical [19], and electrical [20] stimuli. However, these tunable metasurfaces require high operating power and exhibit slow response time and weak modulation in amplitude.

Recently, it has been shown that transparent conducting oxide (TCO) materials provide advantages for designing various tunable plasmonic and nanophotonic devices [21-28]. By applying a relatively low electric field across the insulator-TCO-metal interface, an accumulation layer of charge carriers near the interface is formed, thus leading to a large refractive index change in the accumulation layer of the TCO for efficient optical modulation [29-34]. Since the drift velocity of electrons to form the accumulation layer is fast (exceeds THz), with the small footprint and low capacitance of nano-devices, the modulation speed could easily exceed tens of GHz [27, 30].

In this paper, we propose a novel compact and flat color filter based on metasurface heterostructure in which the light transmission can be electrically controlled. The proposed structure is a modified periodic metal-insulator-metal (MIM) configuration with ultrathin layers of indium tin oxide (ITO) and hafnium dioxide (HfO_2) sandwiched between two gold nanostrips. When electrically biased, the ITO layer changes its optical property due to the formation of an electron accumulation layer at the ITO-HfO_2 interface and hence changing the resonant property of the structure. The numerical simulation shows that a high modulation ratio of 20.5 dB of transmission can be achieved near the epsilon-near-zero (ENZ) region, where the permittivity of the ITO approaches zero. Moreover, the structure exhibits the maximum resonance shift of 40 nm under 5 V bias. The scheme opens up the tantalizing opportunity of designing next generation tunable, ultra-compact, and efficient wavelength selective filters.

The schematic of the proposed color filter is depicted in Fig. 1. A subwavelength nano-slit array is patterned on the top of the SiO_2

substrate with period p. Inspired by the MIM plasmonic structure, the nanostrip with width w consists of two gold layers and an active ITO layer sandwiched between two HfO_2 insulation spacers. The thicknesses of Au and HfO_2 layers are 90 nm and 5 nm, respectively. The thickness of the ITO (H_{ITO}) is designed from 30-100 nm. In this design, the insulting HfO_2 layer allows a voltage bias up to 5V without electrical breakdown [30, 35]. The refractive index of SiO_2 is modeled with the standard Sellmeier expansion[36] whereas that of Au and HfO_2 are taken from experimental data[37].

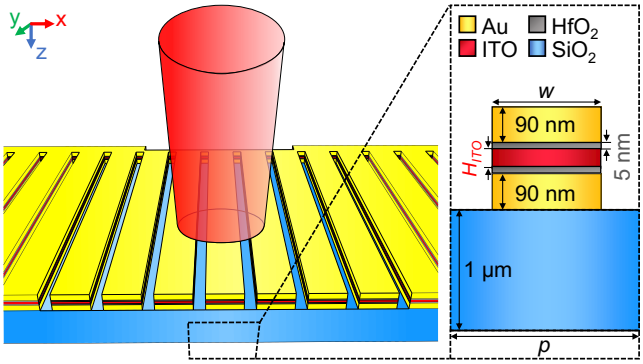

Fig. 1. Schematic of the proposed tunable color filter. Inset: Cross-section of the unit element of the designed structure.

We numerically studied the optical response of the color filter using the Finite Element Method (FEM) (COMSOL Multiphysics). To find the dependence of the transmission peak on the structural parameters, we performed parametric sweeps on the period and width of the nanostrip. The ITO layer thickness was fixed at H_{ITO} = 30 nm, and the slit width was defined as $s = p - w$. The incident light with transverse magnetic (TM) polarization (i.e. electric field polarized parallel to the x-axis in Fig. 1) was used. The wavelength-dependent transmission properties of the color filter varied with the period (p: 500 nm -1000 nm) and fixed slit width (s = 90 nm) as shown in Fig. 2 (a). It can be seen in the figure that a decrease in the cavity width results in an increase of transmission efficiency. As shown in Fig. 2 (b), the scanning is conducted by increasing the slit width s from 50 nm to 200 nm but keeping p = 800 nm. From the simulation, we can see the transmission peak redshifts linearly as the period slit width increases or decreases. In addition, the bandwidth of the resonant peak slightly narrows down as the slit width decreases. Since the plasmonic resonance condition is directly related to the period (p) and the slit width (s) of the nanostrip array, therefore, by carefully selecting the geometric factors such as period and slit width of the nanostrip array, one can achieve a desired transmission peak position and efficiency [38]. Nevertheless, a tradeoff between transmission efficiency and transmission peak bandwidth should be considered in practical structure design. Since operating wavelength, we are interested in, is telecommunication wavelength band, the period and width of the nanostrip array will be kept as 800 nm and 710 nm, respectively. Thus configured, filter will provide a transmission peak at 1540 nm.

Figure 3 depicts the electric field profile and z-component magnetic field profile of the color filter at the peak wavelength of 1540 nm. The electric distribution shows a superposition of E_x and E_y, forming a current loop inside the MIM layer and thereby denotes the character of the magnetic resonance, which is reconfirmed in Fig. 3 (b) by the strong confinement of the magnetic field in the gap region between the two gold strips. Due to the high confinement of the plasmonic resonance, modifying the material in the gap region could lead to a strong change of the transmission properties.

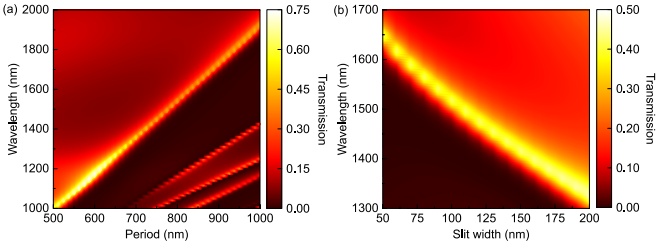

Fig. 2. Transmission properties of the optical filters with varying geometric factors. (a) Map of transmission spectra with varying period p of the structure. The slit width is kept constant as 90 nm. (b) Map of transmission spectra for varying slit width s of the structure. The period is kept constant as 800nm.

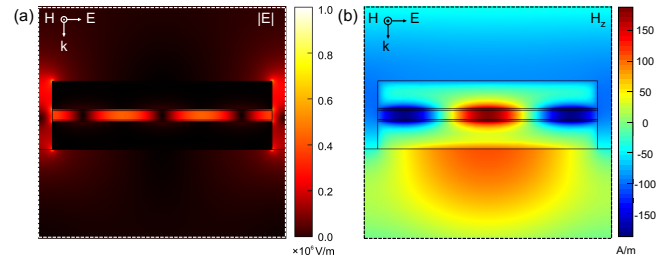

Fig. 3. (a) Electric field distribution and (b) z-component magnetic field distribution for a filter structure with p = 800 nm, s = 90 nm, and TM polarization incidence light at wavelength of 1540 nm

Integration of TCO material (i.e., ITO) into the MIM filter provides such tunability via field-effect dynamics. To determine the characteristics of these tunable filtering properties, we first simulated the carrier concentrations and charge profiles of the ITO corresponding for different gating voltages (Fig. 4 (a), (b)). Identical biases were applied to the top and bottom gold strips and the ITO layer was grounded. Numerical simulations of the electron concentration distributions were carried out using electronic solver (DEVICE, Lumerical Solutions) [39]. The device simulator uses the finite element method to self-consistently solve the Poisson and drift-diffusion equations. In our electronic simulations, we used a self-adaptive mesh generation algorithm with a maximum of 20,000 refinement steps and a minimum mesh size of 5×10^{-4} nm.

The frequency dependent ITO permittivity $\epsilon_{ITO}(\omega)$, can be described with the Drude model as [30]

$$\varepsilon_{\mathrm{ITO}}(\omega) = \varepsilon_{\infty} - \frac{\omega_p^{\,2}}{\omega^2 + i\omega\Gamma} \quad \text{where} \quad \omega_p = \sqrt{\frac{Ne^2}{(\varepsilon_0 m^*)}}. \quad \textbf{(1)}$$

Here, ϵ_∞, ω_p, and Γ stand for the permittivity at infinite frequency, plasma frequency, and the electron relaxation rate respectively. The plasma frequency relates to the carrier concentration N, effective electron mass m^*, and electron charge e. The values of the parameters are $\epsilon_\infty = 3.9$, $\Gamma = 2\times10^{14}$ rad/s, and $m^* = 0.28\times m_0$ where m_0 is electron rest mass [40].

By applying a positive bias through the gold and ITO layer, an accumulation layer of electrons is formed at the HfO_2-ITO interface, thus changing the carrier distribution. Figure 4 (c) shows the corresponding carrier concentration N versus the position from HfO_2-ITO interface under different biases.

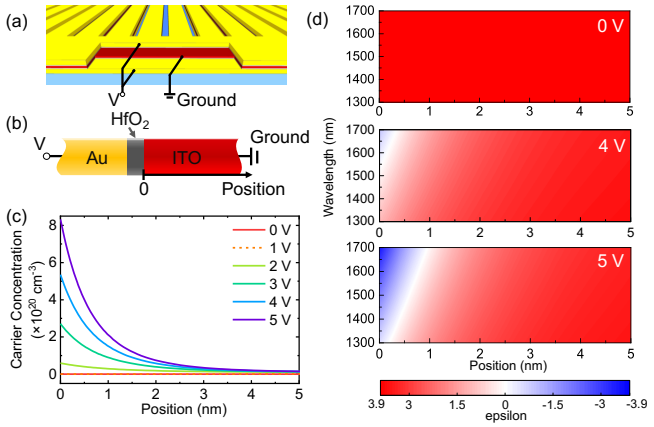

Fig. 4. (a) Configuration for field-effect modulation for the proposed structure. (b) Metal-oxide-TCO structure used to simulate the electric and optical properties of the ITO accumulation layer. (c) Simulated carrier concentration distribution of the ITO layer at the first 5 nm range from the ITO-HfO_2 interface. (d) Corresponding real part permittivity distribution of the ITO as a function of wavelength for 0 V (top), 4 V (middle), and 5 V (bottom). The permittivity is calculated with a standard Drude model for the ITO material.

The spatial distribution of the real part of ITO permittivity versus wavelength for different applied voltages is shown in Fig. 4 (d). Without the applied voltage, the permittivity near the HfO_2-ITO interface is close to 3.9, which indicates that the ITO acts as a dielectric material ($\epsilon_{ITO} > 0$). As the applied voltage increases to 5 V, the permittivity decreases to a negative value and hence exhibits metallic properties ($\epsilon_{ITO} < 0$). The ENZ region where the permittivity of the ITO approaches near zero could be observed when applying bias (i.e. white region for $\epsilon_{ITO} = 0$ in Fig.4 (d)). Therefore, by applying the bias and coupling to the ENZ region, the electric field distribution in the proposed optical filter, as well as the transmission properties, will be altered.

Next, we simulated the transmission of the color filter by introducing field effect modulation of the ITO material. Figure 5 (a) shows the transmission spectra for different voltage biases from 0 V to 5 V with a step size of 0.5 V. Under low bias, an obvious resonant peak shift can be observed, indicating the change of resonant properties of the structure due to the formation of the accumulation layer. As the bias is gradually increased, more electrons concentrate on both interfaces, and thus the permittivity decreases in these two accumulation layers. Once the ENZ wavelength range (an e.g. white region in Fig. 4 (d)) approaches to the resonant wavelength of the structure through the voltage application, the resonant mode will couple to the ENZ mode [27, 30]. The coupling of the plasmonic resonance and the ENZ resonance can result in damping and hence leading to lower transmission (e.g. 4-5 V in Fig. 5 (a)). The substantial reduction of simulated transmission efficiency above 4 V is consistent with the formation of the ENZ layer in Fig. 4 (d). It is also worth noting that the resonance peak presents a shift under bias as shown in the inset of Fig. 5 (a). Two different regimes can be observed relating to the modification of the resonance. For a positive bias below 4 V, transmission peak shows blueshift due to the decrease of permittivity with applied bias. In contrast, the peak redshifts under a bias higher than 4 V. This is because negative permittivity of the ITO is formed near the interface, making the region metallic. As a consequence, the effective thickness of the ITO in the resonant cavity is shrunk which leads to a shift of the transmission peak to a longer wavelength.

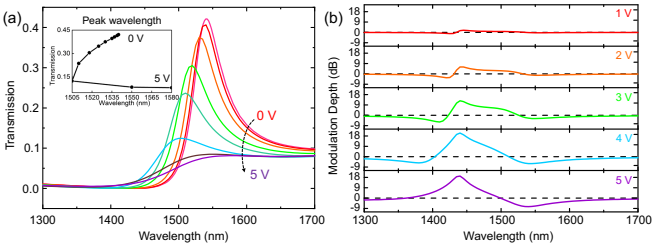

Fig. 5. Simulation results of the structure under bias. (a) Transmission spectrum from 0 V to 5 V with 0.5 V step. (Inset) The corresponding peak for each spectrum. (b) Modulation value of the proposed structure from 1 V to 5 V with 1 V step size.

To have a further insight into the effect, modulation depth MD (dB) = 10 × log (T_v/T_0) was calculated as shown in Fig. 5 (b) for a bias from 1 V to 5 V with a step size of 1 V. T_v and T_0 refers to the transmission with the applied bias and without bias, respectively. Clearly, the modulation strength reaches 20.5 dB and 20.3 dB for 4 V and 5 V bias, respectively, representing a strong modulation near the resonant wavelength.

The *y*-component electric field inside the nanostrip at 1540 nm is shown in Fig. 6 for illustration of the modulating performance. When no bias is applied, as plotted in Fig.6 (a), the electric field at two cavity edges is antiparallel to each other, because the ITO layer and the HfO_2 layer behave as the dielectric cavity in this case. Enlarged field profiles near the top HfO_2-ITO interface under 0 V, 4 V, and 5 V are shown in Fig. 6 (b), (c) and (d) respectively. The inset shows the magnified field profile and the corresponding permittivity distribution of the ITO within a 2 nm area from the interface. Under 4 V and 5 V bias, as the permittivity decreases to zero, an electric field is enhanced in the accumulation layer due to the continuity of the normal component of electric displacement (i.e. $\epsilon_{\perp}E_{\perp}$) through the interface, which is caused by the coupling of ENZ resonance. Furthermore, the permittivity of the ITO at 5 V is negative at the interface leading to a negative field intensity distribution. This can be seen from Fig. 6 (d), the field distribution agrees well with the epsilon distribution in the accumulation layer. Therefore, the significant change in transmission is due to the ENZ coupling which modifies the resonance properties of the structure.

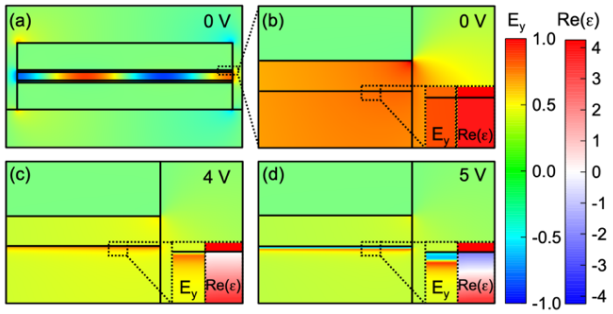

Fig. 6. (a) *Y*-component electric field profile of nanostrip area under 0 V. The zoom-in field profiles near HfO_2-ITO interface region under bias (b)0 V, (c)4 V and (d)5 V.

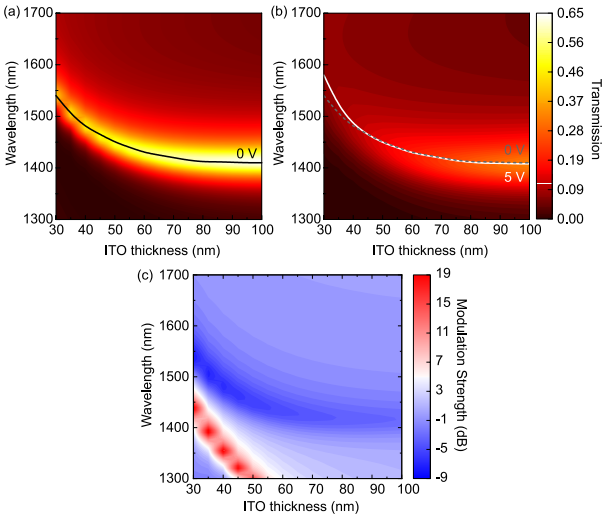

Fig. 7. Map of transmission spectra for varying ITO layer thicknesses under an applied bias of (a) 0 V and (b) 5 V. The solid curve relates to transmission peak position under 0 V and 5 V in (a) and (b), respectively. The transmission peak at 0 V in (a) is replotted in (b) (dashed black curve) as a reference to illustrate peak shifting. (c) Map of modulation strength for different ITO layer thicknesses at 5 V applied bias.

Finally, to further analyze the role of the accumulation layer in modifying resonance, we investigated the transmission spectra with different ITO layer thicknesses ranging from 30 nm to 100 nm under 0 V and 5 V bias. From Fig. 7, taking the non-bias condition as an example, the resonance first shifts to shorter wavelength, then remains around 1425 nm with the increases of the ITO thickness. The shifting regime for the thin ITO layer (< 50 nm) can be attributed to the resonance condition of the propagating plasmonic mode since the plasmonic resonance is sensitive to the cavity length. For the thicker ITO layer, larger cavity length leads to a lower quality factor and widening the transmission bandwidth. When we compared the 5 V bias to the 0 V bias (Fig. 7 (a), (b), (c)), the modulation worked for all ITO layer thicknesses. Since the thickness of the accumulation layer is relatively small (Debye length ~2-3 nm, Fig. 4 (c)), the modulation strength could be enhanced with thinner ITO thicknesses since the plasmonic confinement is comparable with the thickness of the formed accumulation layer.

In conclusion, we demonstrated electro-optical tuning in a metasurface color filter composed of MIM heterostructure nanostrip arrays. By carefully choosing geometrical parameters, a desired resonant peak can be realized. The ITO layer inside gold strips enables electro-optical modulation of transmission properties which manifests in altering the transmission efficiency and shifting the transmission peak position with external bias. The structure leads to a modulation strength exceeding 20 dB with 4 V voltage bias. An electrically-modulated nanoscale color filter could be the basis for novel applications in imaging, display, and optical/bio-sensing devices.

Funding. This work was supported in part by National Science Foundation (CAREER Award Program, Grant Number 1752295); Robert A. Welch Foundation (Award number: AA-1956-20180324); Young Investigator Development Program and the Office of the Vice Provost for Research at Baylor University.

Acknowledgment. J.Z. acknowledges the support from China Scholarship Council (CSC). A.A. acknowledges the Office of the Vice Provost for Research at Baylor University for the postdoctoral research fellowship.

References

1. A. V. Kildishev, A. Boltasseva, and V. M. Shalaev, Science **339**, 1232009 (2013).
2. N. Yu and F. Capasso, Nat. Mater **13**, 139 (2014).
3. M. Khorasaninejad, F. Aieta, P. Kanhaiya, M. A. Kats, P. Genevet, D. Rousso, and F. Capasso, Nano Lett **15**, 5358 (2015).
4. Q. Wang, X. Zhang, Y. Xu, Z. Tian, J. Gu, W. Yue, S. Zhang, J. Han, and W. Zhang, Adv. Opt. Mater **3**, 779 (2015).
5. L. Cong, S. Tan, R. Yahiaoui, F. Yan, W. Zhang, and R. Singh, Appl. Phys. Lett **106**, 031107 (2015).
6. L. Xie, W. Gao, J. Shu, Y. Ying, and J. Kono, Sci. Rep **5**, 8671 (2015).
7. N. Yu, F. Aieta, P. Genevet, M. A. Kats, Z. Gaburro, and F. Capasso, Nano Lett **12**, 6328 (2012).
8. F. Ding, Z. Wang, S. He, V. M. Shalaev, and A. V. Kildishev, ACS Nano **9**, 4111 (2015).
9. G. Li, M. Kang, S. Chen, S. Zhang, E. Y. Pun, K. W. Cheah, and J. Li, Nano Lett **13**, 4148 (2013).
10. W. Yue, S. Gao, S.-S. Lee, E.-S. Kim, and D.-Y. Choi, Laser Photonics Rev **11**, 1600285 (2017).
11. O. Wolf, S. Campione, J. Kim, and I. Brener, Opt. Express **24**, 21512 (2016).
12. Y. Horie, A. Arbabi, E. Arbabi, S. M. Kamali, and A. Faraon, Opt. Express **24**, 11677 (2016).
13. D. Fleischman, L. A. Sweatlock, H. Murakami, and H. Atwater, Opt. Express **25**, 27386 (2017).
14. S. Yokogawa, S. P. Burgos, and H. A. Atwater, Nano Lett **12**, 4349 (2012).
15. S. P. Burgos, S. Yokogawa, and H. A. Atwater, ACS Nano **7**, 10038 (2013).
16. P. Gutruf, C. Zou, W. Withayachumnankul, M. Bhaskaran, S. Sriram, and C. Fumeaux, ACS Nano **10**, 133 (2016).
17. J. Sautter, I. Staude, M. Decker, E. Rusak, D. N. Neshev, I. Brener, and Y. S. Kivshar, ACS Nano **9**, 4308 (2015).
18. M. Rahmani, L. Xu, A. E. Miroshnichenko, A. Komar, R. Camacho-Morales, H. Chen, Y. Zárate, S. Kruk, G. Zhang, D. N. Neshev, and Y. S. Kivshar, Adv. Funct. Mater **27**, 1700580 (2017).
19. M.-X. Ren, W. Wu, W. Cai, B. Pi, X.-Z. Zhang, and J.-J. Xu, Light Sci. Appl **6**, e16254 (2017).
20. T. Kan, A. Isozaki, N. Kanda, N. Nemoto, K. Konishi, M. Kuwata-Gonokami, K. Matsumoto, and I. Shimoyama, Appl. Phys. Lett **102**, 221906 (2013).
21. V. E. Babicheva, A. Boltasseva, and A. V. Lavrinenko, Nanophotonics **4,** (2015).
22. X. Liu, J. H. Kang, H. Yuan, J. Park, S. J. Kim, Y. Cui, H. Y. Hwang, and M. L. Brongersma, Nat. Nanotechnol **12**, 866 (2017).
23. M. Abb, B. Sepulveda, H. M. H. Chong, and O. L. Muskens, J. Optics **14**, 114007 (2012).
24. K. F. Shi, R. R. Haque, B. Y. Zhao, R. C. Zhao, and Z. L. Lu, Opt. Lett. **39**, 4978 (2014).
25. K. F. Shi and Z. L. Lu, Opt. Commun **370**, 22 (2016).
26. K. F. Shi, R. R. Haque, W. S. Zhao, R. C. Zhao, and Z. L. Lu, Proc. SPIE **8980**, 898012 (2014).
27. H. W. Lee, G. Papadakis, S. P. Burgos, K. Chander, A. Kriesch, R. Pala, U. Peschel, and H. A. Atwater, Nano Lett **14**, 6463 (2014).
28. G. Kafaie Shirmanesh, R. Sokhoyan, R. A. Pala, and H. A. Atwater, Nano Lett **18**, 2957 (2018).
29. Z. Lu, K. Shi, and P. Yin, MRS Advances **1**, 1657 (2016).
30. Y. W. Huang, H. W. Lee, R. Sokhoyan, R. A. Pala, K. Thyagarajan, S. Han, D. P. Tsai, and H. A. Atwater, Nano Lett **16**, 5319 (2016).
31. A. Forouzmand and H. Mosallaei, IEEE T Nanotechnol **16**, 296 (2017).
32. J. Park, J.-H. Kang, S. J. Kim, X. Liu, and M. L. Brongersma, Nano Lett **17**, 407 (2016).
33. F. Yi, E. Shim, A. Y. Zhu, H. Zhu, J. C. Reed, and E. Cubukcu, Appl. Phys. Lett **102**, 221102 (2013).
34. J. Park, J. H. Kang, X. Liu, and M. L. Brongersma, Sci. Rep **5**, 15754 (2015).
35. A. Anopchenko, L. Tao, C. Arndt, and H. W. H. Lee, ACS Photonics **5**, 2631 (2018).
36. G. P. Agrawal, "Nonlinear fiber optics," in *Nonlinear Science at the Dawn of the 21st Century* (Springer, 2000), pp. 195.
37. E. D. Palik, *Handbook of optical constants of solids* (Academic Press, 1998), Vol. 3.
38. H. W. Gao, W. Zhou, and T. W. Odom, Adv. Funct. Mater **20**, 529 (2010).
39. "DEVICE", retrieved https://www.lumerical.com/tcad-products/device/.
40. V. Vm and V. Fistul, Sov, Phys. Semicond+ **4**, 1278 (1971).

Full References

1. A. V. Kildishev, A. Boltasseva, V. M. Shalaev, Planar photonics with metasurfaces. *Science* **339**, 1232009 (2013).
2. N. Yu, F. Capasso, Flat optics with designer metasurfaces. *Nature Materials* **13**, 139-150 (2014).
3. M. Khorasaninejad, F. Aieta, P. Kanhaiya, M. A. Kats, P. Genevet, D. Rousso, F. Capasso, Achromatic metasurface lens at telecommunication wavelengths. *Nano Letters* **15**, 5358-5362 (2015).
4. Q. Wang, X. Zhang, Y. Xu, Z. Tian, J. Gu, W. Yue, S. Zhang, J. Han, W. Zhang, A broadband metasurface-based terahertz flat-lens array. *Advanced Optical Materials* **3**, 779-785 (2015).
5. L. Cong, S. Tan, R. Yahiaoui, F. Yan, W. Zhang, R. Singh, Experimental demonstration of ultrasensitive sensing with terahertz metamaterial absorbers: A comparison with the metasurfaces. *Applied Physics Letters* **106**, 031107 (2015).
6. L. Xie, W. Gao, J. Shu, Y. Ying, J. Kono, Extraordinary sensitivity enhancement by metasurfaces in terahertz detection of antibiotics. *Scientific Reports* **5**, 8671 (2015).
7. N. Yu, F. Aieta, P. Genevet, M. A. Kats, Z. Gaburro, F. Capasso, A broadband, background-free quarter-wave plate based on plasmonic metasurfaces. *Nano Letters* **12**, 6328-6333 (2012).
8. F. Ding, Z. Wang, S. He, V. M. Shalaev, A. V. Kildishev, Broadband high-efficiency half-wave plate: A supercell-based plasmonic metasurface approach. *ACS Nano* **9**, 4111-4119 (2015).
9. G. Li, M. Kang, S. Chen, S. Zhang, E. Y. Pun, K. W. Cheah, J. Li, Spin-enabled plasmonic metasurfaces for manipulating orbital angular momentum of light. *Nano Letters* **13**, 4148-4151 (2013).
10. W. Yue, S. Gao, S.-S. Lee, E.-S. Kim, D.-Y. Choi, Highly reflective subtractive color filters capitalizing on a silicon metasurface integrated with nanostructured aluminum mirrors. *Laser & Photonics Reviews* **11**, 1600285 (2017).
11. O. Wolf, S. Campione, J. Kim, I. Brener, Spectral filtering using active metasurfaces compatible with narrow bandgap III-V infrared detectors. *Optics Express* **24**, 21512-21520 (2016).
12. Y. Horie, A. Arbabi, E. Arbabi, S. M. Kamali, A. Faraon, Wide bandwidth and high resolution planar filter array based on DBR-metasurface-DBR structures. *Optics Express* **24**, 11677-11682 (2016).
13. D. Fleischman, L. A. Sweatlock, H. Murakami, H. Atwater, Hyper-selective plasmonic color filters. *Optics Express* **25**, 27386-27395 (2017).
14. S. Yokogawa, S. P. Burgos, H. A. Atwater, Plasmonic color filters for CMOS image sensor applications. *Nano Letters* **12**, 4349-4354 (2012).
15. S. P. Burgos, S. Yokogawa, H. A. Atwater, Color imaging via nearest neighbor hole coupling in plasmonic color filters integrated onto a complementary metal-oxide semiconductor image sensor. *ACS Nano* **7**, 10038-10047 (2013).
16. P. Gutruf, C. Zou, W. Withayachumnankul, M. Bhaskaran, S. Sriram, C. Fumeaux, Mechanically tunable dielectric resonator metasurfaces at visible frequencies. *ACS Nano* **10**, 133-141 (2016).
17. J. Sautter, I. Staude, M. Decker, E. Rusak, D. N. Neshev, I. Brener, Y. S. Kivshar, Active tuning of all-dielectricmetasurfaces. *ACS Nano* **9**, 4308-4315 (2015).
18. M. Rahmani, L. Xu, A. E. Miroshnichenko, A. Komar, R. Camacho-Morales, H. Chen, Y. Zárate, S. Kruk, G. Zhang, D. N. Neshev, Y. S. Kivshar, Reversible thermal tuning of all-dielectric metasurfaces. *Advanced Functional Materials* **27**, 1700580 (2017).
19. M.-X. Ren, W. Wu, W. Cai, B. Pi, X.-Z. Zhang, J.-J. Xu, Reconfigurable metasurfaces that enable light polarization control by light. *Light: Science & Applications* **6**, e16254 (2017).
20. T. Kan, A. Isozaki, N. Kanda, N. Nemoto, K. Konishi, M. Kuwata-Gonokami, K. Matsumoto, I. Shimoyama, Spiral metamaterial for active tuning of optical activity. *Applied Physics Letters* **102**, 221906 (2013).
21. V. E. Babicheva, A. Boltasseva, A. V. Lavrinenko, Transparent conducting oxides for electro-optical plasmonic modulators. *Nanophotonics* **4**, 165–185 (2015).
22. X. Liu, J. H. Kang, H. Yuan, J. Park, S. J. Kim, Y. Cui, H. Y. Hwang, M. L. Brongersma, Electrical tuning of a quantum plasmonic resonance. *Nature Nanotechnology* **12**, 866-870 (2017).
23. M. Abb, B. Sepulveda, H. M. H. Chong, O. L. Muskens, Transparent conducting oxides for active hybrid metamaterial devices. *Journal of Optics* **14**, 114007 (2012).
24. K. F. Shi, R. R. Haque, B. Y. Zhao, R. C. Zhao, Z. L. Lu, Broadband electro-optical modulator based on transparent conducting oxide. *Optics Letters* **39**, 4978-4981 (2014).
25. K. F. Shi, Z. L. Lu, Field-effect optical modulation based on epsilon-near-zero conductive oxide. *Optics Communications* **370**, 22-28 (2016).
26. K. F. Shi, R. R. Haque, W. S. Zhao, R. C. Zhao, Z. L. Lu, Tunable plasmonic metamaterial based on transparent conducting oxide. *Physics and Simulation of Optoelectronic Devices XXii* **8980**, 898012 (2014).
27. H. W. Lee, G. Papadakis, S. P. Burgos, K. Chander, A. Kriesch, R. Pala, U. Peschel, H. A. Atwater, Nanoscale conducting oxide PlasMOStor. *Nano Letters* **14**, 6463-6468 (2014).
28. G. Kafaie Shirmanesh, R. Sokhoyan, R. A. Pala, H. A. Atwater, Dual-Gated Active Metasurface at 1550 nm with Wide (> 300°) Phase Tunability. *Nano Letters* **18**, 2957-2963 (2018).
29. Z. Lu, K. Shi, P. Yin, Photonic MOS Based on “Optical property inversion”. *MRS Advances* **1**, 1657-1669 (2016).
30. Y. W. Huang, H. W. Lee, R. Sokhoyan, R. A. Pala, K. Thyagarajan, S. Han, D. P. Tsai, H. A. Atwater, Gate-tunable conducting oxide metasurfaces. *Nano Letters* **16**, 5319-5325 (2016).
31. A. Forouzmand, H. Mosallaei, Real-time controllable and multifunctional metasurfaces utilizing indium tin oxide materials: A phased array perspective. *IEEE Transactions on Nanotechnology* **16**, 296-306 (2017).
32. J. Park, J.-H. Kang, S. J. Kim, X. Liu, M. L. Brongersma, Dynamic reflection phase and polarization control in metasurfaces. *Nano Letters* **17**, 407-413 (2016).
33. F. Yi, E. Shim, A. Y. Zhu, H. Zhu, J. C. Reed, E. Cubukcu, Voltage tuning of plasmonic absorbers by indium tin oxide. *Applied Physics Letters* **102**, 221102 (2013).
34. J. Park, J. H. Kang, X. Liu, M. L. Brongersma, Electrically tunable epsilon-near-zero metafilm absorbers. *Scientific Reports* **5**, 15754 (2015).
35. A. Anopchenko, L. Tao, C. Arndt, H. W. H. Lee, Field-effect tunable and broadband epsilon-near-zero perfect absorbers with deep subwavelength thickness. *ACS Photonics*, **5**, 2631– 2637 (2018).
36. G. P. Agrawal, in *Nonlinear Science at the Dawn of the 21st Century*. (Springer, 2000), pp. 195-211.
37. E. D. Palik, *Handbook of optical constants of solids*. (Academic press, 1998), vol. 3.
38. H. W. Gao, W. Zhou, T. W. Odom, Plasmonic Crystals: A platform to catalog resonances from ultraviolet to near-infrared wavelengths in a plasmonic library. *Advanced Functional Materials* **20**, 529-539 (2010).
39. "Lumerical DEVICE", retrieved https://www.lumerical.com/tcad-products/device/.
40. V. Vm, V. Fistul, Infrared reflection of heavily doped films of In_2O_3. *Sovient Physics Semiconductors-Ussr* **4**, 1278 (1971).